



EO-1 Technology Validation Report

LEISA/Atmospheric Corrector (LAC)

August 4, 2001

Dennis Reuter
NASA/GSFC
Greenbelt, Maryland

NASA/GSFC

TABLE OF CONTENTS

List of Illustrations	iii
List of Tables	iv
1. INTRODUCTION	1
2. TECHNOLOGY DESCRIPTION	1
3. TECHNOLOGY VALIDATION	6
3.1 Ground Test Verification	7
3.2 On-Orbit Test Validation	8
3.2.1 Dark Current Stability	9
3.2.2 Illumination Noise Characteristics	10
3.2.3 Image Quality	12
3.2.4 Absolute Radiometric Calibration and Spectra	12
3.2.5 Colocation with Landsat7	13
3.3 On-Orbit Usage Experience	15
4. SUMMARY AND LESSONS LEARNED	15
5. CONTACT INFORMATION	16
6. REFERENCES	16

LIST OF ILLUSTRATIONS

Figure No.		Page
1	LAC Electronics Module and Optics Module	3
2	Optics Module with Lens Facing Upward...	4
3	Optics Module Details	5
4	Examples of Spectral Line-Shapes Measured with the Monochrometer System	7
5	Summary of Fittings of Measured Normalized Pixel Responses...	8
6	Histogram of DCE Differences	9
7	SNR Ratio as a Function of Wavelength...	10
8	Plot of Row 180 for All Three Arrays Showing the “Fixed Pattern” Noise	11
9	Lunar Image Showing Rise and Fall Distances...	12
10	Two Spectra Obtained in Different Regions Near the Suez Canal	13
11	Overlay of Landsat7 Image on LAC Image Taken Within 1 Minute	14
12	Schematic of EO-1 LAC Data Flow	15

LIST OF TABLES

Table No.		Page
1	Instrument Summary	6

1. INTRODUCTION

The LEISA (Linear Etalon Imaging Spectral Array) Atmospheric Corrector (LAC or AC) on EO-1 is a hyperspectral imager providing 256 channel continuous spectra in the wavelength range from 0.95 to 1.58 microns. It has a single pixel spatial resolution of 250 meters, a 185 km swath-width and a spectral resolving power ($\lambda/\Delta\lambda$) of 200 or greater ($\Delta\lambda < 10$ nm) throughout its spectral range. The imager employs a wedged filter, a sophisticated 2-dimensional filter whose transmission wavelength varies along one of the dimensions, to provide its spectral resolution. The use of the wedged filter greatly simplifies the optical/mechanical design, so that the instrument is adaptable to a wide variety of platforms (i.e. it is a "bolt on" imager).

In this paper we shall present an overview of the camera highlighting its unique features from both a design and data standpoint. We shall discuss the pre-launch instrument characterization process and on-orbit performance. This shall include the use of solar and lunar calibration techniques to obtain absolute radiometric calibration. The application of the data to the problem of atmospheric correction of high-spatial resolution multi-spectral satellite images (e.g. Landsat-type) shall be discussed.

A problem common to all measurements obtained by high-spatial resolution multispectral (MS) imagers aboard satellites is the systematic errors in the apparent surface reflectances caused by atmospheric effects. Temporal and spatial variability in atmospheric scattering and absorption due to aerosols, clouds and molecular species, primarily water vapor, must be accounted for in the retrieval of accurate surface properties. We have developed the moderate spectral/ spatial resolution wedged filter hyperspectral (HS) imager, the LAC, to correct high-spatial, low-spectral resolution MS imagery for atmospheric effects. The spectra it provides may be used to correct images from the Advanced Land Imager (ALI) on EO-1. Because EO-1 is flying in formation one minute behind Landsat 7, the data may be used to correct Landsat 7 also. The LAC provides scientific return both in terms of improved imagery and moderate spatial resolution hyperspectral sensing capabilities. It advances several technologies that are relevant to a number of remote sensing applications.

2. TECHNOLOGY DESCRIPTION

The LAC employs a state-of-the-art wedged infrared filter (a linear variable etalon or LVE) placed in very close proximity to a two-dimensional IR detector array to produce a 2-D spatial image that varies in wavelength along one of the array dimensions. (The LVE is a wedged dielectric film etalon whose transmission wavelength varies along one dimension.) The filter has a nearly linear dependence of wavenumber on position. It has a 0.45 cm section which covers the 1.2 to 1.6 μm spectral region at a resolution of ~ 35 cm^{-1} , and a 0.55 cm section covering the 0.9 to 1.2 μm spectral range at a resolution of ~ 50 cm^{-1} . The sections are bonded together to form a single filter assembly. This filter represents an advance in dielectric thin film technology. Reflective 1/4-wave stacked layers placed on both sides of a 1/2-wave etalon cavity provide the spectral resolution. Out-of-band suppression of the etalon is accomplished with lower resolution filter layers. The wavelength transmitted by all the layers varies as a function of position, thus providing the spectral information.

The two-dimensional spatial image is formed on the array by a small, wide field of view (WFOV) lens. The filter is mounted within 200 μm of the array, so the image is formed simultaneously on the array and the filter. The spectrum of each point of the area imaged is obtained as the orbital motion of the spacecraft scans the image of that area along the focal plane in the variable wavelength dimension.

This creates a three-dimensional spectral map. The spatial resolution is determined by the angular resolution of the imaging optic, the image scan speed and the readout rate of the array. The LAC has a single pixel spatial resolution of $360 \mu\text{radian} \times 360 \mu\text{radian}$ corresponding to a single pixel FOV of $250 \text{ m} \times 250 \text{ m}$ for a 700 km orbit. The LAC uses three identical sub-assemblies in a single module to match the Landsat 7 swath width of 185 km ($\sim 15^\circ$). Each sub-assembly consists of a focal plane formed of a wedged filter mounted to a 256×256 pixel InGaAs detector array placed behind a lens covering a $5^\circ \times 5^\circ$ FOV. The InGaAs detector material was fabricated by Sensors Unlimited of Princeton NJ and were hybridized to a TCM 2620 multiplexer by the Boeing (Rockwell) Science Center in Thousand Oaks CA. Two of the lenses are used off-axis to cover the full 15° so each lens must have a usable $15^\circ \times 5^\circ$ FOV. Thus a single frame consists of an effective focal plane with 768 pixels in the cross-track direction and 256 pixels in the along-track direction. A frame readout rate of approximately 28 Hz matches the image motion caused by the orbital velocity to the interpixel angular separation. That is, the orbital motion of the spacecraft moves the image 1 row in $\sim 0.0356 \text{ s}$. The wedged filter design was chosen for its optical and mechanical simplicity compared to conventional grating, prism, or Fourier transform spectrometers tunable filter systems. As discussed below, this method of obtaining spectra does place some stability constraints on the spacecraft and the scene. The LEISA concept was originally developed at Goddard under the Advanced Technology Insertion Program for the Pluto Fast Flyby Mission[1]. The filters were designed and fabricated by the Optical Coating Laboratories Inc. of Santa Rosa, CA with the aid of test results obtained at Goddard[2,3]. The wedged filter concept has also been developed independently at Hughes Santa Barbara Research Center[4] and their Wedged Imaging Spectrometer (WIS) operating in the visible and near-IR (VNIR) regions has been demonstrated in aircraft flights[5].

The LAC is comprised of two modules, the optics module and the electronics module. Figure 1 shows both modules being tested in the laboratory. The optics module contains the lenses, focal planes and electronics necessary to operate the arrays and to transfer the digitized pixel data to the electronics module. It is mounted to the nadir deck of the spacecraft and bore sighted with the ALI. The electronics module contains the command and data interface to the spacecraft, the array timing and bias circuitry, the thermal electric cooler (TEC) control circuitry and the instrument power supply. It is mounted in a bay below the nadir deck. Because the long-wavelength cut-off of the arrays is $1.6 \mu\text{m}$, they may be operated at near room temperature. However, to decrease the dark current and increase the signal-to-noise ratio, TECs are used to stabilize the array temperatures at $\leq 285 \text{ K}$.

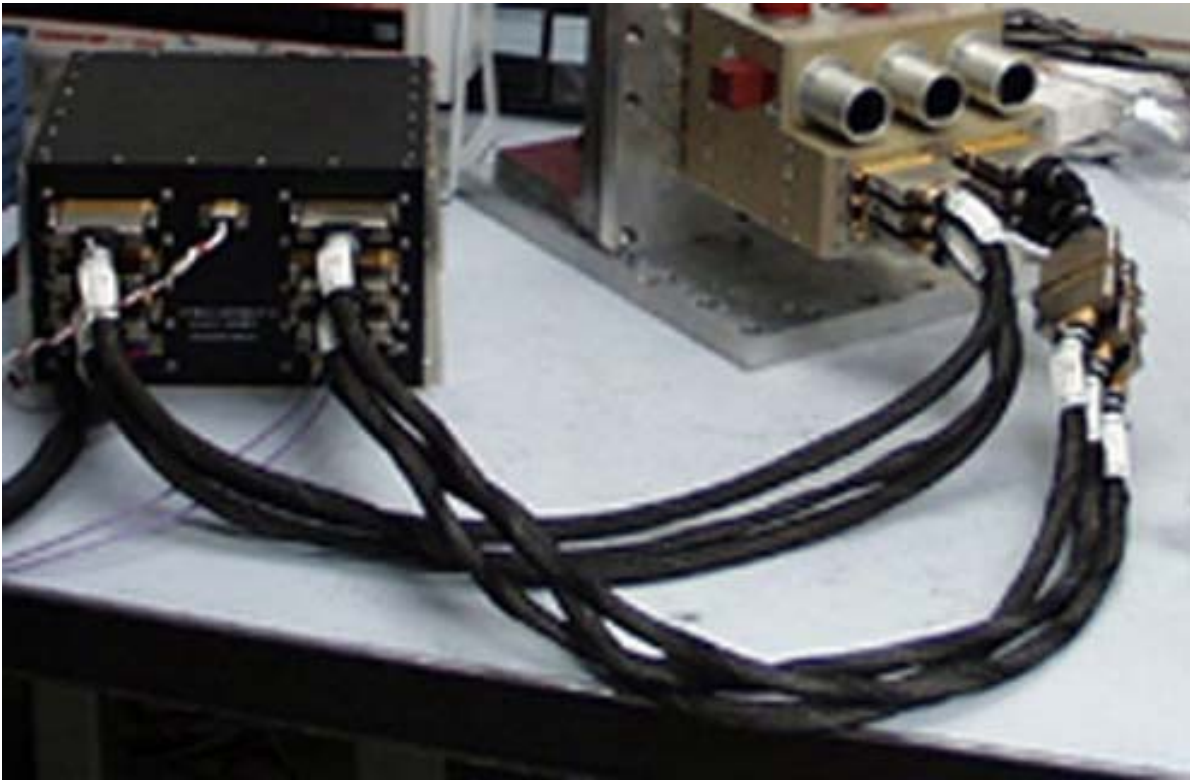


Figure 1. LAC electronics module (left) and optics module. The three lenses are facing outward. The electronic module is 25 cm x 23 cm x 18 cm. The optics module is 19 cm x 18 cm x 14 cm. The cable is separated into two groups of three, one group carrying the analog signals and biases, the other carrying the clock signals.

Figure 2 shows a view of the optics module as it is oriented on the nadir deck. In normal operation the lenses would be facing earthward while the solar calibration tubes would be facing along the direction of the spacecraft motion. During a solar calibration the solar calibration tubes are pointed to within 1° of the sun, and light entering the tubes is reflected off a small spectralon target, providing a reproducible illumination pattern across the focal planes. Because the sun is not imaged through the lenses, it provides only an approximate absolute radiometric calibration. In flight radiometric calibration is provided by lunar scans and by comparisons with the other instruments on EO1 (ALI and Hyperion). Several well-instrumented ground sites are also used for radiometric calibration.

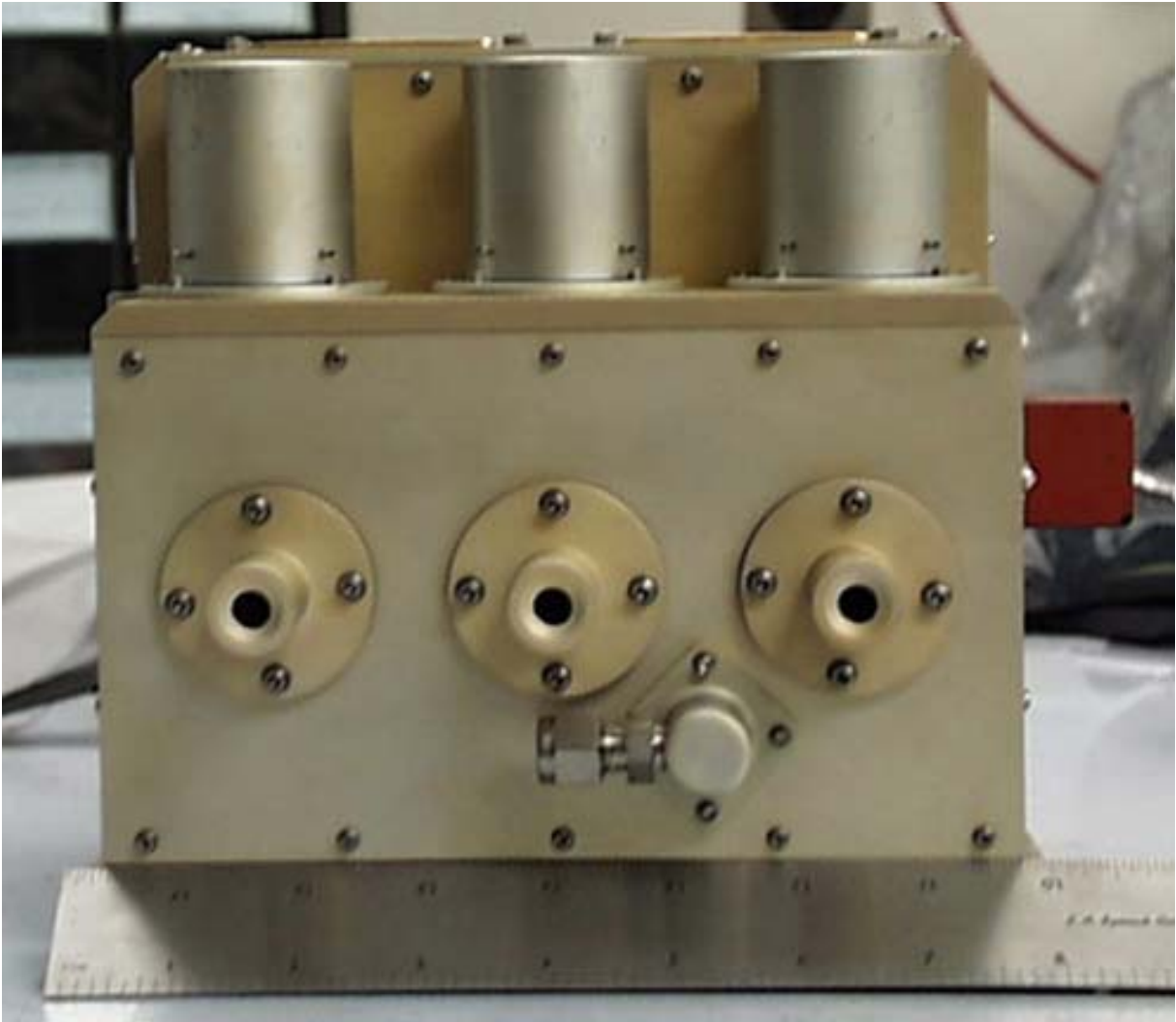


Figure 2. Optics module with lenses facing upward and solar calibration tubes facing forward. The red object to the right is a cover for the optical alignment cube used to align the LAC with the ALI. The fitting in front is an N₂ purge coupling used before launch.

Figure 3 shows the interior detail of the optics module. In normal operation light comes from the right through the triplet lens and is imaged onto the focal planes at the left. The cylinder directly above the focal plane is a stray light baffle. The baffles in the solar calibrators are evident, as is the spectralon reflector. Note that there are three electronics boards, one for each focal plane. The far-left side is mounted to the nadir deck and the TEC heat sinks are mounted to this side. The use of a two module design for the LAC allows a greater degree of flexibility than using a single module. Optical modifications (e.g. wavelength range, resolution etc.) require changes only to the optics module while spacecraft interface changes (e.g. C&DH, power levels etc.) require changes only to the electronics module.

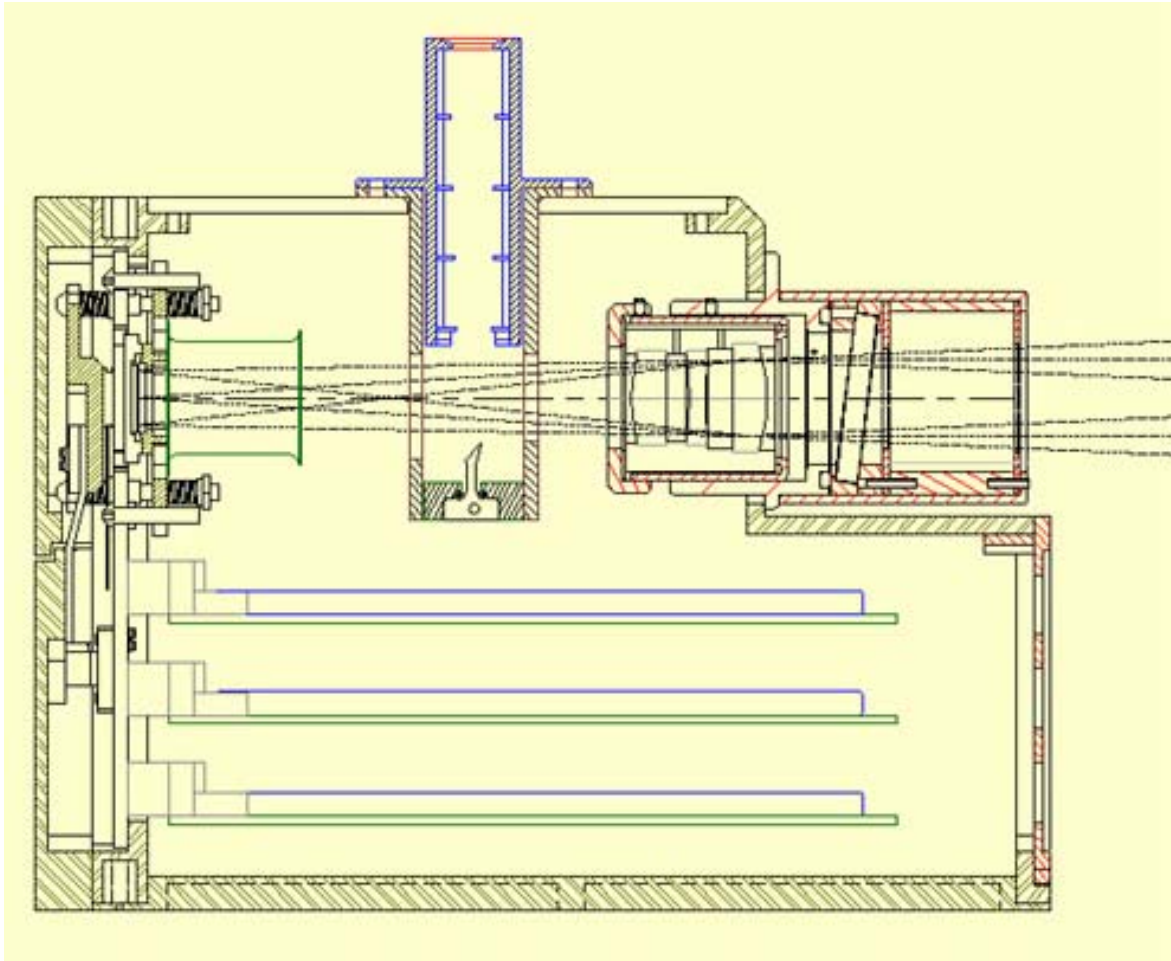


Figure 3. Optics module details. The array/LVE assembly is to the left while light from the scene enters to the right through an air triplet lens. The spectralon target for the solar calibrations is at a 45° angle. The target is sized to approximate a 30 % reflectance surface at 60° solar angle. The tilted element before the lens is a visible/UV reflector.

The LAC has a total mass of 10.5 kg; 4.4 kg for the electronics module, 3.9 kg for the optics module and 2.2 kg for the cable connecting them. It uses a maximum power of 45 W on start-up, which decreases to about 35 W for a TEC temperature setting of 275 K, once the temperature is stabilized. At the nominal frame rate of 28 Hz, which slightly oversamples the spatial dimension in the along-track dimension, the data rate is 95 Mbits/s (12-bit A/D converters are used). A frame rate of 56 Hz allows double sampling in the along-track spatial dimension at the expense of reduced single-frame signal-to-noise ratios. The LAC frame rate could have been adjusted to provide exact single sampling as was done for ALI, however, for simplicity this was not done.

A significant difference between push broom filter imagers such as LAC and ALI and slit imagers such as Hyperion is in the way spectra are formed. In an LVE camera an image is always obtained, however, several images are required to complete the spectrum of a given point in the scene. Thus, excess drift in the image motion can cause a point to cross columns during the acquisition of a full spectrum (see [6] for a discussion of re-sampling in wedged filter spectrometers). Control and

knowledge of the EO-1 spacecraft, and the alignment of the LAC along-track axis to the ALI along-track axis to within 2 arc-minutes, limits this uncertainty to a fraction of a pixel. In the worst case, across-track drift and along-track timing errors lower the effective spatial resolution to 2 pixels, or the Nyquist sampled spatial resolution. In comparison, slit-type imagers obtain all the spectral elements of a given point on the surface simultaneously. In practice, however, off-axis image errors, as well as the effect of oblique incidence for gratings and non-linearity effects for prisms, cause the spectrum to be tilted and/or curved in the focal plane, and thus not to track along a column. These geometric effects are the analog of imperfect sampling in the wedged filter camera, and also cause a loss of effective spatial resolution. A wedged filter camera is inefficient for small sources (e.g. to obtain the spectrum of a point source), it is essentially as efficient as a slit-type instrument for extended sources (e.g. images of the earth's surface from a near earth orbiter). The instrument characteristics of the LAC are summarized in Table 1.

Table 1. Instrument Summary

Type of Spectrometer: Wedged Filter	
Spectral Coverage: 0.89 to 1.58 μm continuous (SNR>10, 0.93 to 1.58 μm)	
Spectral Resolving Power: $\sim 35 \text{ cm}^{-1}$ ($\Delta\lambda$: 5 nm @ 1.2 μm , 9 nm @ 1.6 μm) $\sim 55 \text{ cm}^{-1}$ ($\Delta\lambda$: 4 nm @ 0.9 μm , 8 nm @ 1.2 μm)	
Wavelength Dependence: Linear in Wavenumber (λ^{-1})	
Imaging Optics: Three Multi-Element Refractive, 15° FOV Lenses (f/8, 11.4 cm focal length)	
Dynamic Range: 2048	
Frame Rate: Nominal 27.8 Hz, Maximum 55.6 Hz	
Single Pixel FOV: 0.36 x 0.36 mrad ² (250 x 250 m ² for 705 km orbit)	
Three Array FOV: 264 x 92 mrad ² (185 x 64 km ² for 705 km orbit)	
Memory Required for One 185 x 64 km² Spectral Map: 810 Mbits	
Data Rate: Nominal, 95 Mbits/sec; Maximum, 190 Mbits/sec	
Arrays: 256 x 256 PV InGaAs, 40 μm pixels (TCM 2620 Multiplexer)	
Selectable Focal Plane Temperatures: \sim 285 K, 280 K, 275 K, 265 K	
Power : 48 W peak; 35 W nominal, <10 W orbit average (maximum 20% duty cycle)	
Mass: 10.5 Kg	
<i>Electronics Module</i> (1773 Interface, Power, RS 422 Data Interface, Array Control):	4.4 Kg
<i>Optics Module</i> (Optics, Arrays, Solar Calibrators, TECs, Amplifiers, A/D):	3.9 Kg
<i>Inter-module Cable</i>	2.2 Kg

3. TECHNOLOGY VALIDATION

The primary purpose of the LAC on EO-1 from an orbiting technology validation standpoint was 4-fold: 1) to validate the use of the wedged filter method for obtaining hyperspectral images, 2) to validate the use of a multi-array, multi-telescope system to synthesize a wide-field imager, 3) to validate the use of non-cryogenic InGaAs IR arrays for moderate resolution spectroscopy and to validate the use of lunar and solar measurements (in conjunction with ground-based measurement campaigns) to provide calibration. The science validation was to provide a demonstration of the ability of moderate resolution hyperspectral measurements to provide real-time atmospheric correction information to high-spatial resolution multispectral sounders. This report will not deal with the scientific validation issues.

3.1 GROUND TEST VERIFICATION

Prior to launch, the operational characteristics of the LAC including dark current, read noise, radiometric sensitivity, central wavelength, band-width and angular position were measured for each pixel. The low-illumination noise limit (read noise + dark current) were about 1 – 2 counts while near saturation, in the photon noise limited regime, signal-to-noise ratios of several hundred were obtained. The overall photon to photoelectron conversion efficiency ranged from 0.10 to 0.20. For the most part the characteristics measured prior to launch have not changed with two exceptions: The number of non-responsive pixels has increased since launch and a systematic noise source not apparent in pre-launch tests, and therefore presumably occurring after launch, has modified the radiometric calibration. These effects will be discussed in the next section.

The pre-launch spectral characteristics of each pixel were measured using a grating monochromator whose resolution was much higher than that of the wedged filters. A white light source was imaged onto the entrance slit of the spectrometer and a grating blazed for 12 μm was used to disperse the light. Thus at each grating setting several orders would be present simultaneously, for example, at a 12 μm setting light in orders 13 thru 8 would fall into the 0.92 to 1.6 μm range. The output slit of the monochromator was placed near the focal point of each lens of the LAC, filling each array with collimated light in 5 to 7 orders. Thus, at each grating setting, light would be transmitted at several rows of the array. The central wavelength and band-width of each pixel were determined by stepping the grating in small (1 to 5 nm) increments and fitting the resultant intensity vs. wavelength data to a Gaussian function. Examples of these fittings are shown in Figure 4. As may be seen from this figure, the resolving power of the filter is quite high (e.g. > 200 at 1 μm).

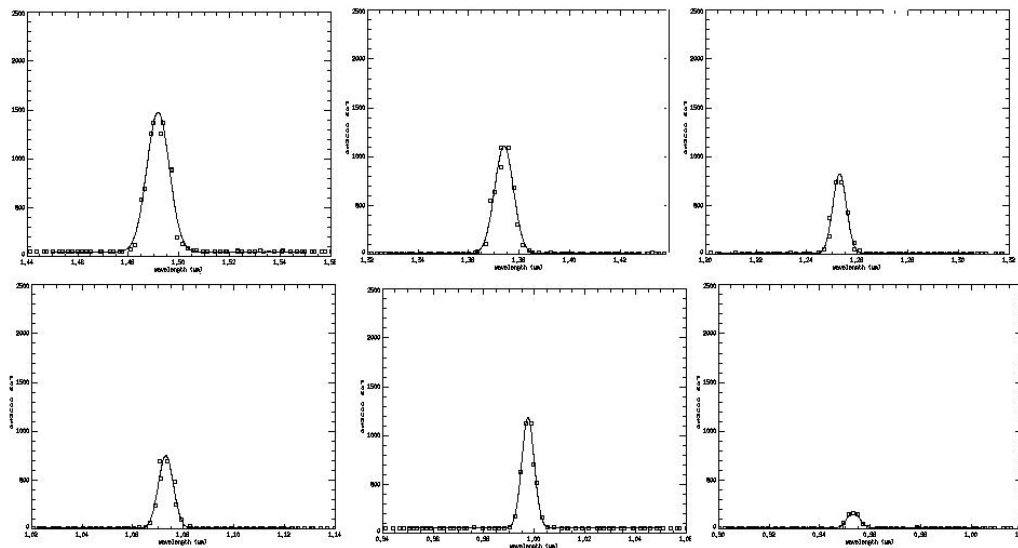


Figure 4. Examples of spectral line-shapes measured with the monochromator system. A Gaussian line-shape was fitted.

In fact, the spectral line-shape at each pixel is closely described by a Gaussian whose full-width at half maximum is 53.34 cm^{-1} for the short-wave filter segment (0.89 to 1.23 μm) and 36.84 cm^{-1} for the long-wave segment (1.21 to 1.58 μm). Figure 5 summarizes the results of fitting Gaussians with a

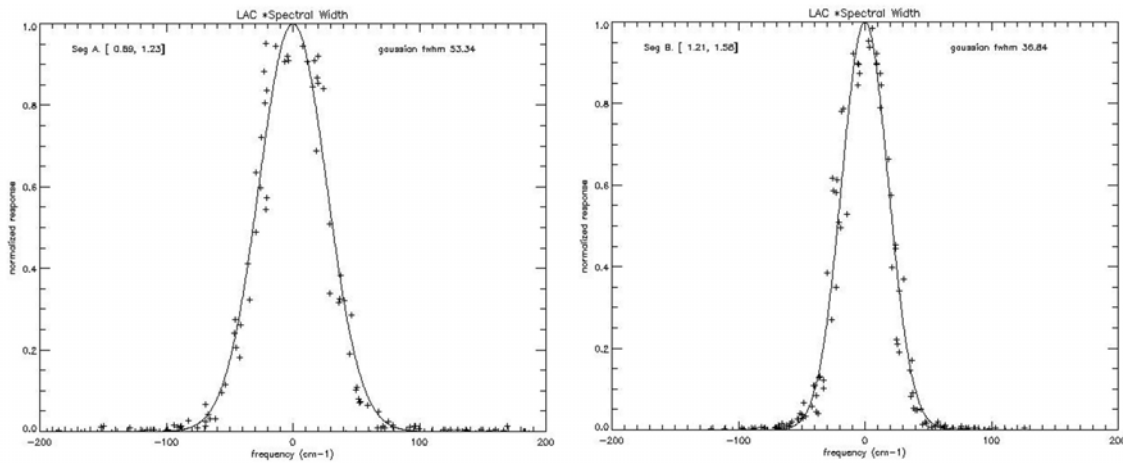


Figure 5. Summary of fittings of measured normalized pixel responses to a single Gaussian function (width in wavenumbers) for the short- (left panel) and long-wavelength filter segments. Pixels covering the entire spectral range are included in the fittings. The constant width in cm^{-1} is consistent with a linear dependence of wavenumber with position on the filter.

single width to normalized intensity vs. wavenumber measurements for several pixels in each filter segment. The wavenumber of each pixel depends nearly linearly on row number.

The angular positions of each pixel in each array were determined relative to an alignment cube attached to the surface of the optics module prior to launch. The measurement was performed using two theodolites. One theodolite was aligned with the surfaces of the cube and used as a transfer standard to determine the angular displacements of the second theodolite. The second theodolite was equipped with a cross-hair target at the focal point of a lens simulating a source at infinity. When re-imaged by the lenses of the LAC, an image of the cross-hair was formed on each of the focal planes. The image of the cross-hair was ~ 20 pixels across, allowing the center of the cross-hair to be located to ~ 0.1 pixel. The image of the cross-hair was translated along the nominal along-track direction of each focal plane by rotating the theodolite source. Position measurements were made at several locations for several rows of each array. In this way, the roll and yaw angles of each array were determined to approximately 40 microradian accuracy (0.1 pixel). This information was used to map the angular position of each pixel for use in geolocating the on-orbit image data. These data were also used to mount the LAC to the nadir deck of the spacecraft in such a way that the yaw angle of the LAC array that overlaps the field-of-view of the ALI was parallel to the ALI yaw angle to within 1 arc-minute. This insured that there was minimal across-track drift (< 0.25 pixel) during a scan.

3.2 ON-ORBIT TEST VALIDATION

On-orbit validation includes: 1) Determining the stability of the arrays under conditions of no illumination, 2) Determining the instrumental noise characteristics under conditions of illumination, 3) Determining the image quality, 4) Determining the absolute radiometric calibration accuracy, 5) Assessing the ability to obtain spectra and 6) Co-locating LAC images with Landsat7 images. A typical on-orbit data collection event (DCE) lasts about 40 seconds during which ~ 1100 frames are obtained at the 28 Hz frame rate (2200 at 56 Hz) and produces a complete spectral image over an area of $\sim 210 \text{ km} \times 185 \text{ km}$. The operation of the instrument is extremely simple. Power is applied to the instrument about 9 minutes before image data is taken to insure the array temperatures and electronics

have stabilized. The frame rate, array temperature set-point and array sensitivity are set by issuing three commands. The data clock is enabled about 8 seconds before the instrument is pointed at the desired surface location to insure that all spectral bands are obtained for the entire target area.

3.2.1 Dark Current Stability

The LAC dark current is measured within 1 orbit of a DCE by imaging a region on the unlit hemisphere of the earth's surface for 1 second (a dark DCE). The average of these dark data is subtracted from each frame of the DCE to remove offsets and dark current at each pixel. The subtraction is done as part of the ground processing of the data. The dark current is very uniform during a dark DCE, with the frame-to-frame standard deviation of each pixel typically being less than 1 count. The dark current is also very stable from day to day, with only a slight drift apparent. This is illustrated in Figure 6 that shows histograms of the differences between a dark DCE on day 198 of 2001 (07/17/01) and two previous dark DCEs (02/27/01 and 04/30/01). From this figure one can see

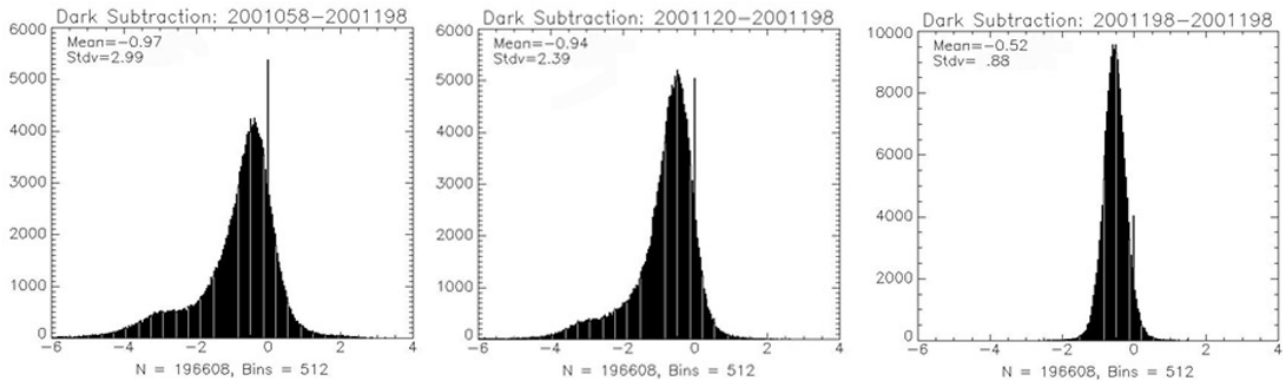


Figure 6. Histogram of difference between a dark DCE on 07/17/01 and dark DCEs on 02/27/01 (leftmost panel), 04/30/01 (center) and a separate dark DCE on 07/17/01. Note the tail of the distribution indicating a slight increase in dark current as a function of time. The rightmost panel shows the difference for two dark DCEs on 07/17/01.

that there is a general broadening of the dark current difference distribution over long periods of time (i.e. weeks) and there appears to be a tendency for the dark current to increase slowly as a function of time. The final panel in the figure shows the reproducibility of the offset on a single day, which is indicative of the error in the offset subtraction methodology. This error of somewhat less than 1 count is the limiting error in the low illumination case. The bias of 0.5 counts in the last panel is representative of the array temperature control stability.

The slow broadening of the dark current distribution is probably related to an observed slight increase in non-responsive pixels since launch. At launch there were about 400 non-responsive pixels (~ 0.2% of the total) and in the 8 months since then another 1100 have been added (for a total of ~0.8%). Typically this number grows at a rate of 1/day, however on two occasions several hundred pixels have “died” within a single DCE. (Note: Since the instrument is turned off between DCEs it is possible the pixel mortality could have occurred at any time since the turn-off after the previous DCE and the beginning of data at the current DCE). There were no other operational (e.g. radiation, solar cell overvoltage etc.) or instrumental (e.g. overvoltage, excess current, etc.) anomalies at these times and the cause of the increased non-responsive pixels is still being investigated. It has had no major operational effect since the relative number of pixels affected is still quite small (<1%) and they are scattered throughout the arrays. Prior to launch the arrays were damaged by contact with the wedged

filter holders during a vibration test. The contact was caused by an incorrect assembly procedure, which was subsequently corrected, and no further damage was observed in additional vibration testing. However, gradual long-term effects on the multiplexer bump bonds from this incident remains a strong candidate for the cause of the pixel mortality.

3.2.2 Illumination Noise Characteristics

The limit on the signal-to-noise ratio (SNR) under most illumination conditions is determined by the Poisson distributed statistical variance of the photon flux from the source. The solar calibration DCEs are used to evaluate to assess this limit for the LAC, since the illumination is constant. The standard deviation of each pixel is measured over the 200 frames obtained during the calibration and the ratio of this to the average signal is used to determine the SNR. Figure 7 shows a wavelength dependent

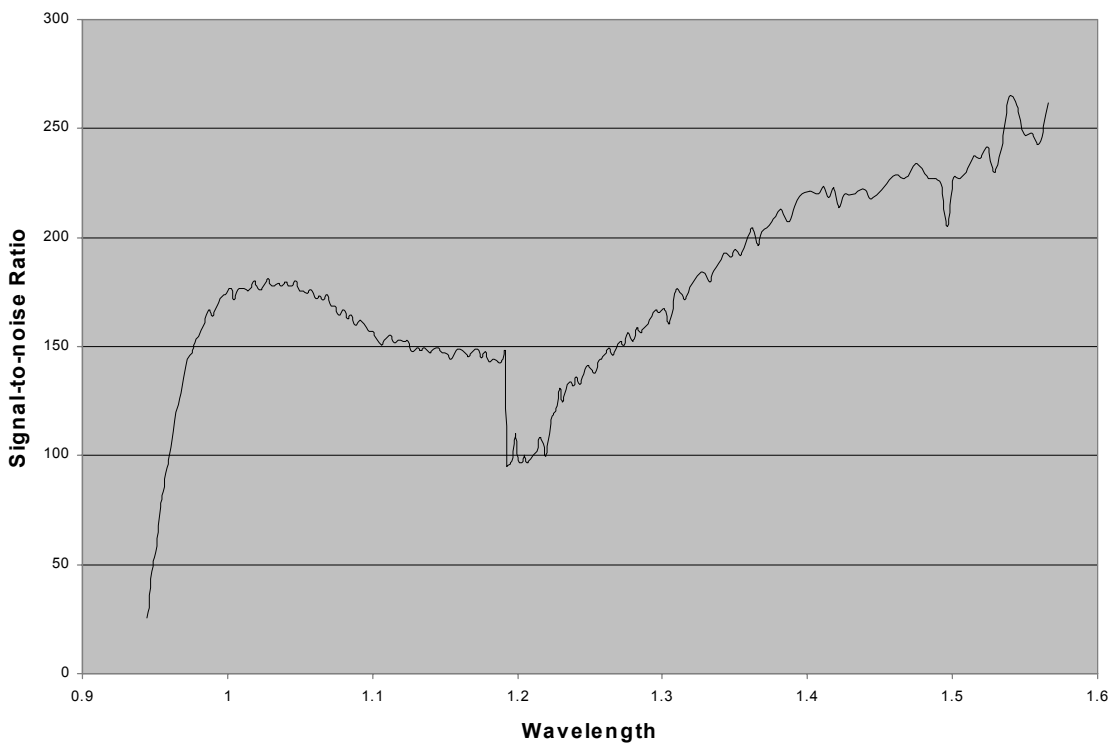


Figure 7. SNR ratio as a function of wavelength determined from a solar calibration DCE in the method described in the text. The rapid drop-off shortward of 0.97 μm is caused by loss of quantum efficiency in the InGaAs arrays.

summary of the SNR obtained in this fashion. The discontinuity at $\sim 1.2 \mu\text{m}$ marks the boundary between the two filter segments. Note that the SNR is greater than 100 everywhere, consistent with pre-launch calculations. In fact, since the solar calibration level is only about 25% of the maximum before saturation is reached, the maximum SNR ratio is expected to be about a factor of 2 higher than shown here. However, as discussed below, a systematic noise source that apparently occurred after launch limits the actual SNR to values lower than shown in Figure 7. Since digital saturation occurs well before the actual analog detector saturation (digital saturation occurs at about 20% of the 2.5 million electron detector element full well), the signals do not show large non-linearities near saturation.

As mentioned above, the actual LAC noise is dominated by a systematic source that appeared after launch. Initially, it was very difficult to obtain images not showing excessive pixel-to-pixel variation (streaking) at nearly the 10 % level. The source of this streaking was found only after a scanning solar calibration showed that for most illumination levels there was a relatively constant “fixed pattern” noise that did not appear in the dark frames. In a scanning solar calibration, the solar calibration tubes are nodded $\pm 6^\circ$ about the solar direction varying the amount of light scattered off the spectralon target in a non-calibrated, but uniform way. This maneuver was initially performed to assess the stability of illumination during a solar calibration, and not as an additional calibration method. Figure 8 shows a plot of a typical row of all three arrays for several positions of the solar calibration tubes. The offset has been subtracted in this plot. Two observations immediately present themselves: 1) for

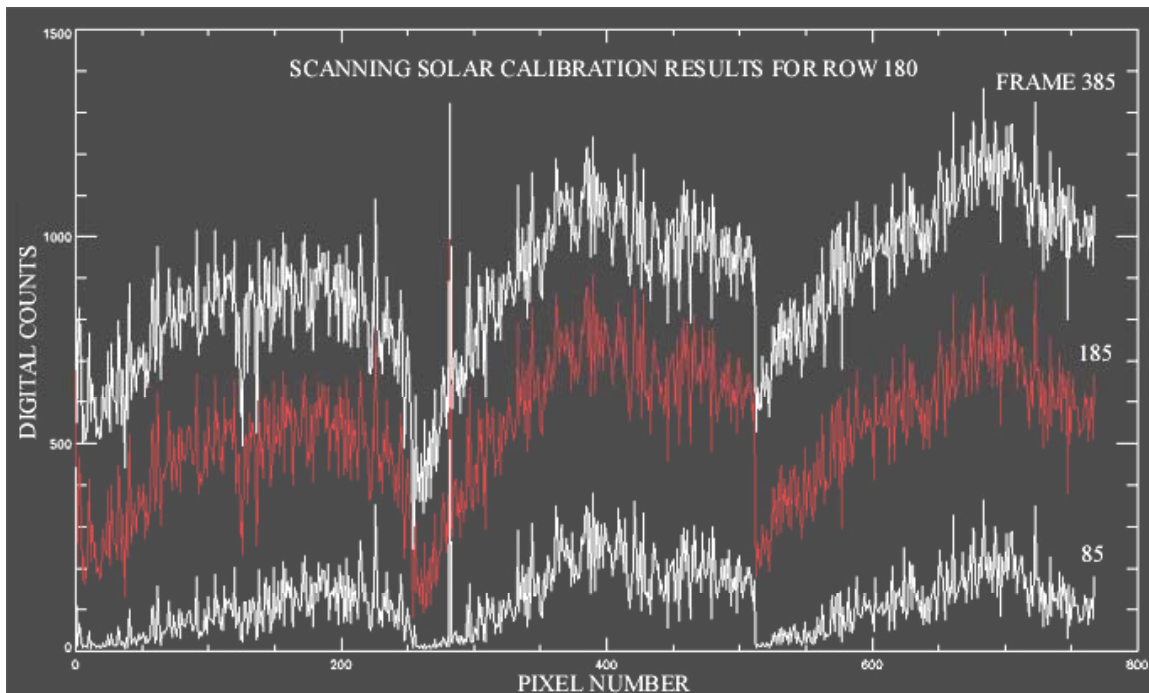


Figure 8. Plot of row 180 for all three arrays showing the “fixed pattern” noise. As the pointing of the solar calibration tubes is rolled about the solar position, the array illumination varies from a maximum in frame 385.

most illumination levels there is a large, relatively illumination independent pixel-to-pixel variation which 2) does not decrease the number of counts below the dark level (i.e. there are no large negative numbers in the differences). Data from the scanning solar calibrations are now used in the calibration method to account for this “fixed pattern” noise. That it is very reproducible for a given illumination level is evidenced by the nearly photon noise limited variance of the signal from any given pixel during a non-scanning solar DCE (e.g. Figure 7). Unfortunately, one irreversible effect of this noise is that once the resultant of the illumination and the noise combines to give the same output count as the offset level, further reductions in illumination do not lower the output level. Thus, there are uncorrectable non-linearities at low illumination levels. Prior to launch, the only time all spacecraft systems could be operated was during thermal vacuum testing and the “fixed pattern” noise was not seen in LAC data from the last illuminated test carried out at that time. Since subsequent LAC tests were carried out in non-illuminated conditions, all that may be said is that this noise appeared sometime between the last thermal vacuum test and the first on-orbit DCE. The most likely causes of this systematic noise component are: 1) although the thermal-vacuum tests were designed to closely

simulate orbital conditions it is possible that there is a system interference that was not present in these simulations, 2) launch vibration could have altered the LAC and 3) power supply filter components that were stressed by an overvoltage condition during the conducted susceptibility test may have failed. The causes are still being investigated.

3.2.3 Image Quality

Prior to launch the image quality was checked by imaging a simulated source at infinity onto a single pixel. The on-orbit terrestrial surface images indicate that the focus has remained good after launch. As a further test, images of the moon obtained during the lunar calibration scans have been used to determine the rise distance of a sharp boundary. The results, as illustrated in Figure 9, show a rise from 5% illumination to 95% illumination in approximately 1 pixel, again indicating excellent focus and image quality.

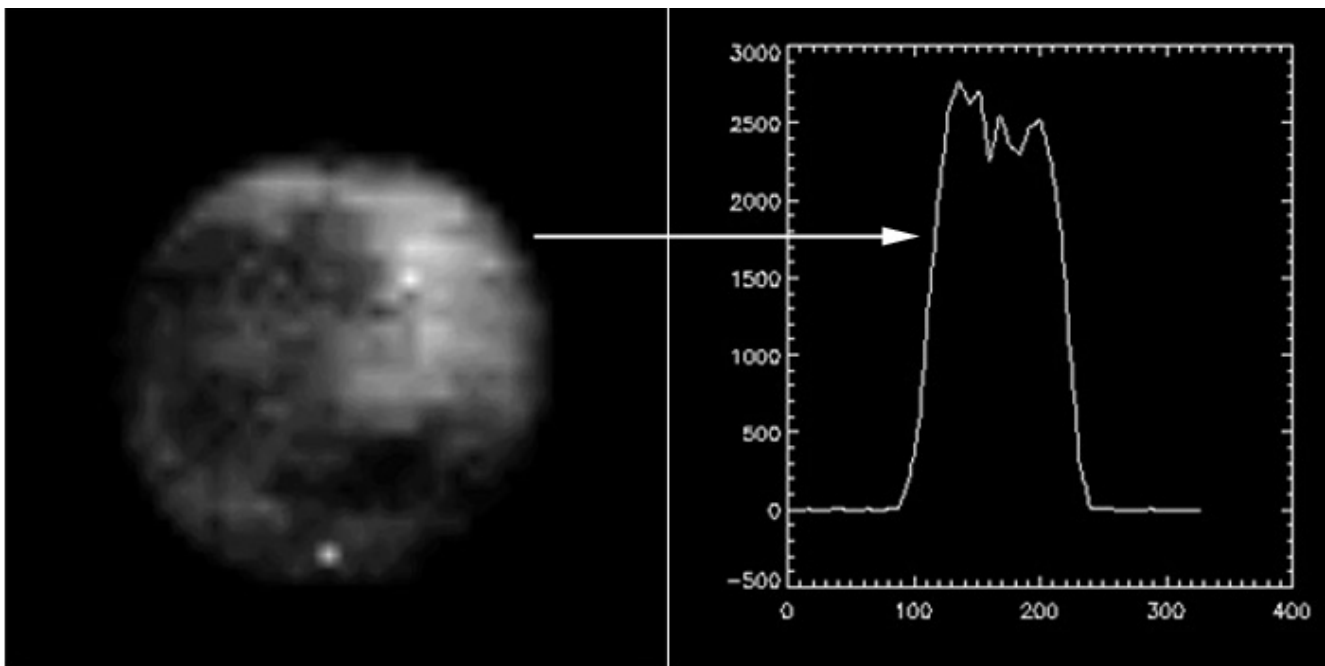


Figure 9. Lunar image (expanded by a factor of 8) showing rise and fall distances (5% to 95%) of 8 to 10 pixels (on expanded scale), indicating single pixel imaging capability. Without expansion the moon fills about 20% of an array (~ 25 pixels).

3.2.4 Absolute Radiometric Calibration and Spectra

Because of the relatively recent identification of the “fixed pattern” noise in the images, the absolute radiometric calibration is still proceeding. The ability to create spectra is illustrated in Figure 10 that shows two spectra obtained in Suez. The differing water vapor absorption is clearly visible here.

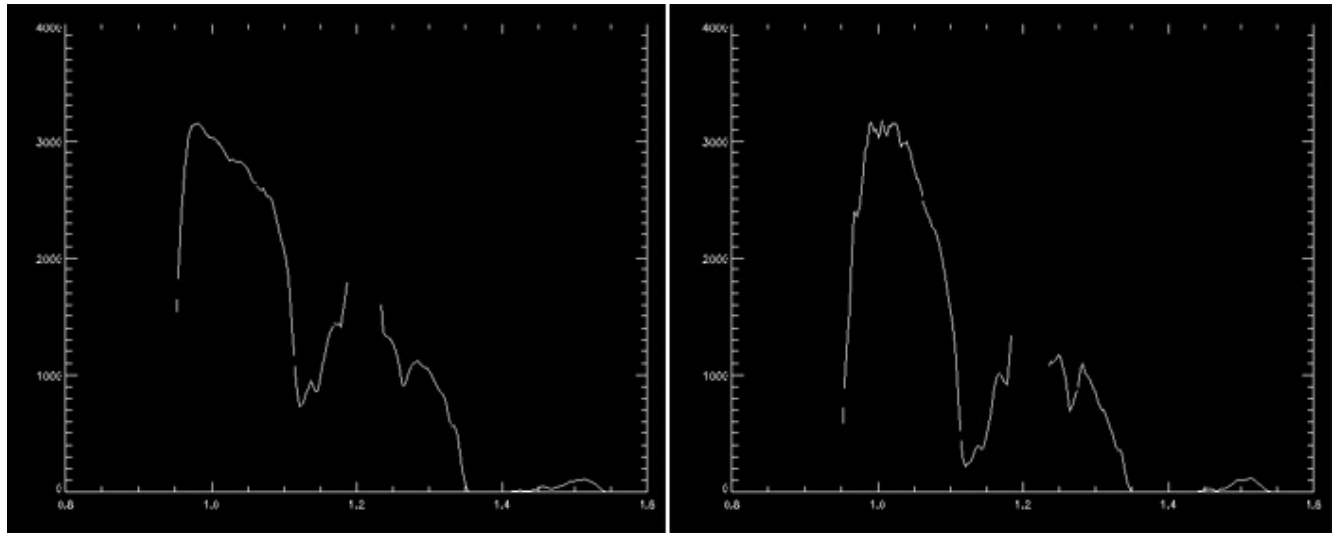


Figure 10. Two spectra obtained in different regions near the Suez Canal. Note the much deeper absorption at 1.13 μm in the right panel, indicative of greater atmospheric water vapor.

3.2.5 Co-location with Landsat7

As part of the data processing single wavelength LAC spectral images are placed on a latitude-longitude grid for comparison with Landsat7 multispectral data. This involves two steps: 1) Using the complete pixel by pixel central wavelength map described in Section 3.1, pixels within $\frac{1}{2}$ resolution element of a desired wavelength are selected. The angular position of these pixels is taken from the position map also described in Section 3.1, 2) The angular positions are projected onto a surface latitude-longitude map using the spacecraft attitude information provided as part of the ancillary data on each data tape. As shown in figure 11, this process produces accurately positioned maps, further verifying the pre-launch angular measurements. The potential utility of the LAC for correcting Landsat7 data is illustrated here, since the real-time atmospheric features are the same in both data sets.

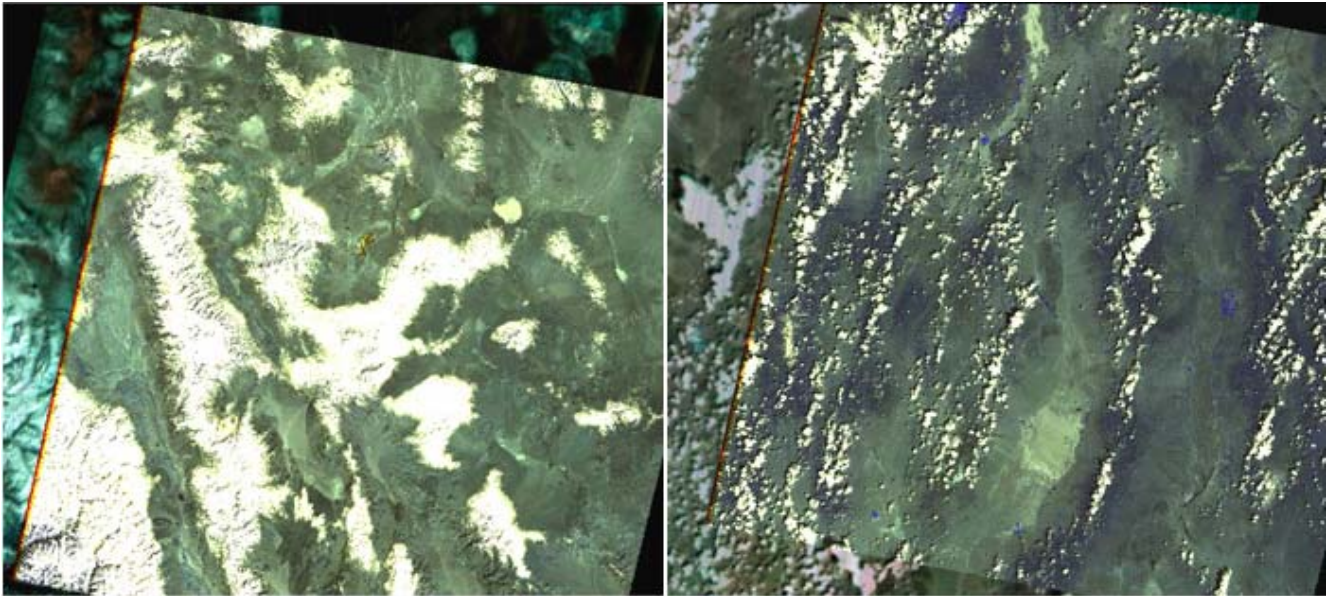


Figure 11. Overlay of Landsat7 image on LAC image taken within 1 minute. Railroad Valley NV (right) and Cuprite CA (left) are used as calibration areas for these instruments. The images are well correlated.

3.3 ON-ORBIT USAGE EXPERIENCE

As of this writing the LAC has obtained approximately 1200 DCE without any instrument failures. As shown diagrammatically in Figure 12, Level 0 image data is received from the GSFC Data Processing Facility (DPF) on tape media and processed to Level 1R (radiometrically calibrated) data at the LAC data processing facility. The Level 1R processing is quite automated and typically takes about 30

Atmospheric Corrector Calibration System

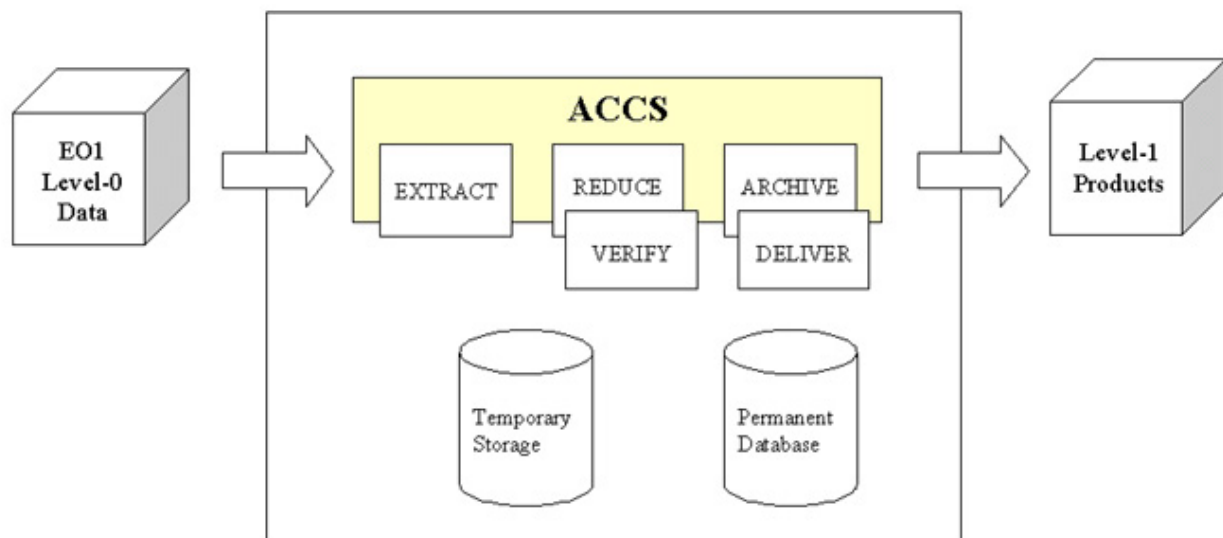


Figure 12. Schematic of EO1 LAC data flow. The ACCS (Atmospheric Corrector Calibration System) is automated for Level 1R radiometrically calibrated data.

minutes per DCE. More highly processed data sets, such as the geo-located data sets, are done on an as needed basis and require more computation time. These processes are currently being automated as well. Data is provided to researchers as requested through the GSFC Science Validation Facility (SVF). Currently, research requests through the EO1 science validation NRA are supported.

4. SUMMARY AND LESSONS LEARNED

The LAC on EO1 has successfully demonstrated a wedged filter hyperspectral imager on a space-based platform. This technology is highly desirable because of its inherent mechanical, electrical and optical simplicity, its low mass and its robust nature because of the total avoidance of moving parts. The two module design allows a wide range of optical design possibilities to be accommodated by changing the lenses or filters and/or arrays in the optics module while keeping the interface and power functions unchanged in the electronics module. Conversely, different spacecraft command and data interface architectures may be accommodated by modifying the electronics module and leaving the optics module unchanged. Although, on first glance, the data produced by imagers of this type are unusual, the data system developed for EO1 produces products identical to those produced by more conventional optical systems. Indeed, the wedged filter system may be used for any application requiring low- to moderate- spectral resolution hyperspectral imaging data, except for those with a rapid temporal variation (i.e. variability on a time scale shorter than that required to scan the

spectrum). The wedged filter system is especially attractive for applications covering a wide wavelength range, but where only segments of the spectrum are needed. In this case, a single array may be used segmenting the wedge to cover only the spectral ranges desired.

The LAC has also demonstrated the utility of space based natural sources for calibration purposes. In future systems the solar calibration tubes will have calibrated off-axis performance characteristics, so that scanning solar calibrations may be used to provide absolute radiometric calibration as well as relative measures. Future atmospheric correctors will also employ InGaAs arrays whose lattice matching InP layers have been thinned to allow shorter wavelength operation. These arrays already exist and would allow operation throughout the visible spectrum, increasing the usefulness for aerosol monitoring.

5. CONTACT INFORMATION

Dr. Dennis C. Reuter
NASA/GSFC
Code 693 (Planetary Systems Branch)
Greenbelt, MD 20771
Phone: 301-286-2042
Fax: 301-286-0212
e-mail: dennis.c.reuter@gsfc.nasa.gov

Mr. George H. McCabe
NASA/GSFC and Catholic University of America
Code 693
Greenbelt MD 20771
Phone: 301-286-8283
Fax: 301-286-0212
e-mail: george.mccabe@gsfc.nasa.gov

6. REFERENCES

- [1] "The Highly Integrated Pluto Payload System (HIPPS): A Sciencecraft Instrument for the Pluto Mission.", S. A. Stern, D. C. Slater, W. Gibson, H. J. Reitsema, Alan Delamere, D. E. Jennings, D. C. Reuter, J. T. Clarke, C. C. Porco, E. M. Shoemaker and J. R. Spencer, *SPIE Proceedings, EUV, X-RAY and Gamma-Ray Instrumentation for Astronomy VI*, **2518**, 39 - 58, San Diego, CA; July 1995.
- [2] "Logarithmically Variable Infrared Etalon Filters." K. P. Rosenberg, K. D. Hendrix, D. E. Jennings, D. C. Reuter, M. D. Jhabvala, and A. T. La, *SPIE Proceedings, Optical Thin Films IV: New Developments*, **2262**, 25 - 27 July, 1994, San Diego, CA.
- [3] "Hyperspectral Sensing Using the Linear Etalon Imaging Spectral Array.", D. C. Reuter, D. E. Jennings, G. H. McCabe, J. W. Travis, V. T. Bly, A. T. La, T. L. Nguyen, M. D. Jhabvala, P. K. Shu and R. D. Endres, *SPIE Proceedings of the European Symposium on Satellite Remote Sensing III: Conference on Sensors, Systems, and Next Generation Satellites II*, **2957**, 154-161, September 23-26, 1996, Taormina, Sicily, Italy.

- [4] G. T. Elerding, J. G. Thunen and L. M. Woody. "Wedge Imaging Spectrometer: application to drug and pollution law enforcement.", *SPIE Vol. 1479, Surveillance Technologies*, Orlando, FL; April 1991.
- [5] L. M. Woody and J. C. Dermo. "Wedge Imaging Spectrometer (WIS) hyperspectral data collections demonstrate sensor utility.", *International Symposium on Spectral Sensing Research (ISSR) 1994*, San Diego, CA; July 1994.
- [6] "Observations Using the Airborne Linear Etalon Imaging Spectral Array (LEISA): A 1- to 2.5-micron Hyperspectral Imager for Remote Sensing Applications", G. McCabe, D. C. Reuter, SC. Tsay, P. L. Coronado, D. E. Jennings, P. K. Shu, P. Mantica, S. Cain, M. Abrams, Arthur L. Boright and J. L. Ross, *SPIE Proceedings of the European Symposium on Satellite Remote Sensing VI: Conference on Sensors, Systems, and Next Generation Satellites V*, September 20-24, 1999, Florence, It.